ELSEVIER

Journal of Molecular Catalysis A: Chemical 184 (2002) 311–322

JOURNAL OF MOLECULAR CATALYSIS A: CHEMICAL

www.elsevier.com/locate/molcata

CO_2 reforming of CH_4 over Rh-containing catalysts

U.L. Portugal [a], A.C.S.F. Santos [b], S. Damyanova [c], C.M.P. Marques [d], J.M.C. Bueno [b,*]

[a] *Departmento de Engenharia Quimica, Universidade Federal de Santa Maria, 97105900 Santa Maria, RS, Brazil*
[b] *Departmento de Engenharia Quimica, Universidade Federal de São Carlos, Caixa Postal 676, 13565-905 São Carlos, SP, Brazil*
[c] *Institute of Catalysis, Bulgarian Academy of Sciences, 1113 Sofia, Bulgaria*
[d] *DQ, Universidade Federal de São Carlos, Caixa Postal 676, 13565-905 São Carlos, SP, Brazil*

Abstract

Two series Rh catalysts were prepared depending on the kind of the support: (i) Rh supported on zeolite and (ii) on oxide carriers. Rh/NaY zeolite catalysts were prepared by ion-exchange from an aqueous solution of $[Rh(NH_3)_5]Cl_3$. Rh catalysts supported on γ-Al_2O_3, Nb_2O_5 and TiO_2 were prepared by incipient wetness impregnation method of the carrier with an aqueous solution of $RhCl_3{\cdot}2H_2O$. The catalysts were characterized by X-ray diffraction (XRD) spectroscopy, nuclear magnetic resonance (NMR), temperature-programmed desorption of hydrogen (TPD-H_2). Test reaction for Rh catalysts was CO_2 reforming of methane at different reaction temperatures. TPD data showed that the dispersion of metal particles depends on the pretreatment activation procedure; highest dispersion was observed for samples previously calcined and then activated in H_2. Catalysts activated directly in H_2, steam or submitted directly to the reaction conditions showed large metal particles. The effect of the protons on the destabilization of the zeolite framework during reaction was revealed by the higher Si/Al ratios, due to a dealumination of the zeolite. Neutralization of protons with solution of NaOH leaded to a stabilization of the dispersion and zeolite structure. Correlation between the dispersion and specific activity in CO_2 reforming was found for zeolite-supported Rh catalysts. When the activities are compared by turnover frequencies, oxide-supported Rh catalysts are significantly more active compared to zeolite-supported ones due to a higher degree of participation of the reverse water–gas shift reaction (WGSR). The difference in activity and thermal stability was related to the nature of the support.

Keywords: Rhodium catalysts; Zeolite; Oxides; CO_2 reforming of CH_4; XRD; TPD; ^{29}Si NMR

1. Introduction

The catalytic process of carbon dioxide reforming of methane to synthesis gas, which converts two of the most abundant and cheapest carbon-containing gases (CH_4 and CO_2) into a useful chemical products, has received considerable attention in recent years [1–6]. This reaction offers important advantages: (i) the formation of a suitable H_2/CO ratio for use in a Fischer–Tropsh synthesis to liquid carbons [7], (ii) reducing of CO_2 and methane emissions as both gases are contributors to the greenhouse effect [8] and (iii) better use in the chemical energy transmission [9].

The research of the catalysts for this reaction has been mainly focused on the intrinsic activity of the metal phase, on its stability towards carbon formation, the type of the support most suitable for improving the efficiency of the catalyst and the reaction mechanism.

* Corresponding author.
E-mail address: jmcb@power.ufscar.br (J.M.C. Bueno).

1381-1169/02/$ – see front matter
PII: S1381-1169(02)00018-3

Although the extensively development of catalysts based on non-noble metals (Fe, Co or Ni) from the industrial point of view, these catalysts have shown very high activity, which is completely lost within a few hours of reaction, that is due to the formation of a stable and inactive carbon on the surface [10–13]. Because of this, recently numerous studies related to the reforming of methane with carbon dioxide were focused over noble metal catalysts supported on different carriers, which exhibit better activity and very high stability due to the less sensitivity to carbon deposition [14,15] compared to non-noble metal catalysts. Rostrup-Nielsen [15] comparing catalysts based on nickel, ruthenium, rhodium, palladium, iridium and platinum has found that ruthenium and rhodium showed high selectivity for carbon-free operation. It has been found that the performance of Rh catalysts under reaction conditions of CO_2 reforming of methane strongly depends on the carrier employed to disperse the metal. The initial specific activity, the deactivation rate, and the carbon deposition were found to depend on the support material. Zhang et al. [16] showed that three main factors are contributed to the catalyst deactivation of Rh catalysts supported on different carriers: (i) carbon deposition, (ii) sintering of metal crystallites and (iii) blocking of the Rh surface sites by species originating from the carrier, as the importance of each factor is strongly determined by the nature of the carrier and the size of metal particles.

In our previous work [6], studying ruthenium catalysts supported on zeolite and amorphous carriers in CO_2 reforming of methane, it has been shown that the activity was strongly effected by the activation procedure applied to the catalyst before to be used in the reaction.

In this work we attempted to find a correlation between the activity of Rh-containing catalysts in CO_2 reforming of methane and their structure after different primary treatment. A comparison of the catalytic behavior of rhodium catalysts supported on Y-zeolite and oxide supports such Al_2O_3, TiO_2 and Nb_2O_3 was done. Different techniques were applied for characterization of the samples: X-ray diffraction (XRD), X-ray photoelectron spectroscopy (XPS), ^{29}Si nuclear magnetic resonance (^{29}Si NMR) and temperature-programmed reduction of hydrogen (TPR-H_2).

2. Experimental

2.1. Sample preparation

2.1.1. Zeolite-supported Rh catalysts

NaY was prepared from LZ Y-52 (Si/Al = 2.6, Linde Molecular Sieves) by two successive exchanges with $NaNO_3$, according to the method previously described [17]. Rh/NaY and Rh/NaMOR were prepared by ion-exchange starting from an aqueous solution of $[Rh(NH_3)_5]Cl_3$. The dilute solution of $[Rh(NH_3)_5]Cl_3$ (0.003 M) was slowly added to a stirred zeolite slurry (3 g/l) at 353 K over a period of 12 h, followed by an additional stirring for 60 h. The samples were filtered and washed at room temperature with doubly deionized water until Cl^- free. This followed by drying of the samples at room temperature in air and in a vacuum desiccator for 3 h. The resulting samples were stored in a desiccator over a saturated MH_4Cl solution before to be used. The content of Rh was 3 wt.%.

2.1.2. Amorphous-supported catalysts

Rhodium catalysts supported on γ-Al_2O_3, Nb_2O_5 and TiO_2 were prepared by incipient wetness impregnation method using an aqueous solution of $RhCl_3{\cdot}2H_2O$ with appropriate concentration followed by drying in a rough vacuum at room temperature. The content of Rh was 1–3 wt.%.

2.2. Activation procedure

NaY-supported $[Rh(NH_3)_5(H_2O)]^{3+}$ catalysts before using in test reaction were activated by different procedures:

(A) Sample was heated in a flow of He (100 ml/min) up to 773 K at rate of 2 K/min. This sample was labeled Rh/NaY-A.

(B) Samples were heated up to 653 or 773 K in a flow of pure O_2 (100 ml/min) at a rate of 2 K/min and then maintained at these temperatures for 2 h. After that the samples were cooled to room temperature, followed by reduction in a flow of pure H_2 at 100 ml/min up to 673 K and maintained at this temperature for 2 h. The samples were labeled Rh/NaY-B1 and Rh/NaY-B2 calcined at 653 and 773 K, respectively.

(C) Sample was directly activated under reaction conditions by heating in a mixture of $CH_4/CO_2/N_2$ (20/20/60) from room temperature up to the reaction temperature of 973 K at a rate of 2 K/min in a total flow of 100 ml/min. The sample was labeled Rh/NaY-C.

(D) Sample was activated by a procedure similar to B1, followed by ion-exchange neutralization in two successive treatments with a 1 M aqueous solution of NaOH (pH = 10) at room temperature. The sample was labeled Rh/NaY^{N}-D.

(E) Sample was activated by the procedure similar to B1, after that was exposed to a steam action by heating from room temperature up to 973 K at 2 K/min in a H_2/H_2O/He (5/2.6/92.4) mixture at a total flow rate of 100 ml/min and maintained at this temperature for 2 h. This sample was labeled Rh/NaY^{vap}-E.

(F) Sample was firstly activated by the procedure similar to that described for Rh/NaY^{N}-D and then was exposed to a steam in H_2/H_2O/He (5/2.6/92.4) at 973 K at a total flow of 20 ml/min. The sample was labeled $Rh/NaY^{N,\,vap}$-F.

(G) Sample was activated by the procedure similar to that for Rh/NaY^{N}-D and then exposed to H_2 up to 673 K for 2 h. Sample was labeled Rh/NaY^{N+H_2}-G.

(H) Sample was heated in a H_2 flow of 100 ml/min at a rate of 2 K/min from room temperature up to 673 K and maintained at this temperature for 2 h. The sample was labeled Rh/NaY-H.

Rh supported on Na mordenite was activated by the procedure similar to B1 and was labeled Rh/NaMOR-B1. The neutralized sample was labeled $Rh/NaMOR^{N}$-B1.

Rh catalysts supported on oxide supports, Nb_2O_5, Al_2O_3 and TiO_2, were activated by the procedure E and were labeled $Rh/Nb_2O_5{}^{vap}$-E, $Rh/Al_2O_3{}^{vap}$-E and $Rh/TiO_2{}^{vap}$-E, respectively.

2.3. Characterization

Chemical analysis of the samples was performed by inductively coupled plasma atomic emission spectroscopy (ICP). XPS was performed using a XSAM HS spectrometer from Kratos Analytical. Radiation source was Mg Kα (power given by 15 kV and 15 mA). The pressure in analysis chamber was 10^{-9} Torr. Samples were flooded with low energy electrons from a flood gun to avoid charging effect.

XRD patterns were carried out by a Siemens D-5000 diffractometer using Cu Kα radiation (40 kV, 40 mA) with a Ni filter. Data were collected for the spent catalysts.

^{29}Si MAS NMR spectra were carried out using a Varian Unity Plus 400 MHz spectrometer operating at 9.4 T using 7 mm diameter rotors spinning at 5 kHz. Quantitative spectra were measured at 79.5 MHz with 50° radio-frequency pulses and 30 s recycle delays. Chemical shifts (σ) were given in relation to a tetramethyl-silane (TMS) adjusted for a single ^{29}Si resonance at −91.5 ppm of kaolinite, consistent with the presence of a single Q^3 (OAL) silicon environment [18]. The framework Si/Al ratio from ^{29}Si NMR spectra was determined according to the equation given by Klinowski et al. [19]. The Si/Al ratio accuracy calculated by integrating Gaussian curves was around 5%.

Temperature-programmed desorption of hydrogen (TPD-H_2) analyses of the samples were performed using a Micromeritics Pulse Chemisorb 2705. After activation, samples were exposed to 5% H_2/Ar (30 ml/min) and heated from 298 to 773 K at 10 K/min. Samples were cooled to room temperature for 2 h and purged in Ar for 30 min. The stabilization of H_2 adsorption and of the system was monitored with TCD detector. The samples were cooled to 253 K, then heated from 253 to 873 K at 10 K/min. Error in quantification of the TPD results was estimated at ±3–5%. The amount of H_2 desorbed during TPD analysis was obtained by integration of the TPD profiles and was used to estimate the dispersion of metal particles. The TPD data were expressed as H/Rh molar ratios.

2.4. Reaction

The CO_2 reforming reaction of CH_4 was carried out in a continuous flow quartz tube reactor at 1 atm pressure with a constant feed of composition of $CH_4/CO_2/N_2$ of 20/20/60, respectively at a total flow rate of 100 ml/min, with a 0.05–0.2 g of catalyst. The Rh catalysts were tested in the temperature range of 723–973 K. The Rh/zeolite catalysts were maintained in the reaction conditions for 300 h. The reaction data was monitored after 15 min on stream. The turnover frequencies (TOF) results for oxide-supported

catalysts were calculated in initial time on stream, which was estimated from plot of activity versus time on stream. Reaction products were analyzed by on-line gas chromatography, employing a combination of two GCs (Varian-3400) having a TCD detector. One chromatograph employed He and the other N_2 as carrier gas. For reaction product analysis, two columns of Porapak N and Molecular Sieve 13 X were used in a series-bypass arrangement. TOF and rates (mol_i/s) per number of Rh on surface (mol_{Rh}) were determined under different CH_4 conversions obtained by variation of the total flow rate (Table 3).

3. Results

3.1. XPS results

XPS data of Rh/NaY samples obtained by encapsulating of $[Rh(NH_3)_5(H_2O)]^{3+}$ demonstrate the absence of Cl^- ions.

3.2. XRD spectra

XRD spectra of the Rh/NaY samples after reaction are shown on Fig. 1. For comparison the XRD spectrum of the initial $[Rh(NH_3)_5H_2O]^{3+}$/NaY zeolite presents (Fig. 1a). There is a change of the intensity of XRD peaks of the samples depending on the pretreatment procedure. A small decrease of the intensity of the XRD peaks is observed for samples treated in O_2 at 653 and 773 K followed by heating in H_2, as well as for Rh/NaY^{vap}-E sample (Fig. 1b, c and f). XRD spectrum of the Rh/NaY-C sample submitted to the reaction conditions (Fig. 1d) shows the lowest intensity of the diffraction peaks of the zeolite Y, meaning a partial destruction of the zeolite matrix. Neutralized sample, Rh/NaY^{N}-D, presents XRD patterns similar to those of the initial NaY zeolite that suggests a higher degree of preserved crystalline (Fig. 1e).

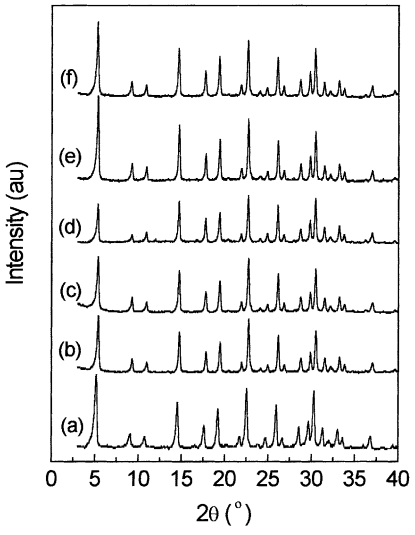

Fig. 1. XRD spectra for zeolite-supported Rh samples treated by different activation procedures: $[Rh(NH_3)_5(H_2O)]^{3+}$/NaY zeolite (a); Rh/NaY-B1 (b); Rh/NaY-B2 (c); Rh/NaY-C (d); Rh/NaY^{N}-D (e); Rh/NaY^{vap}-E (f).

3.3. TPD-H_2 results

TPD data (H/Rh) for all samples are listed in Table 1. It is seen from Table 1 that the different activation procedures have a significant effect on the particle size of the catalysts. The samples previously calcined at different temperatures and then reduced by hydrogen show the highest H/Rh ratios of 1 and 0.98, respectively for Rh/NaY-B1 and Rh/NaY-B2. This indicates a high dispersion of metal particles. After neutralization of the protons with NaOH the Rh/NaY^{N}-D and Rh/NaY$^{N+H_2}$-G samples have also a high H/Rh of 0.90. Non-neutralized sample after treatment in the steam, Rh/NaY^{vap}-E, shows a significant decrease of the H/Rh ratio from 1.0 to 0.42, as well as the neutralized sample exposed to H_2O/H_2, Rh/NaY$^{N,\,vap}$ (Table 1). The Rh/NaY-B1 and neutralized, Rh/NaY^{N}-D, samples after reaction show slowly decrease of the H/Rh ratio (0.86 and 0.85, respectively), suggesting that the dispersion of Rh particles, practically does not significantly change during reforming of CH_4. However, the sample submitted directly to the conditions of the reaction, Rh/NaY-C, shows very low H/Rh of 0.18. The zeolite-supported $[Rh(NH_3)_5(H_2O)]^{3+}$ complex after heating in He undergoes extensive autoreduction leading to a formation of large metal particles (Table 1). It has been shown [20] that the heating of $[Rh(NH_3)_5(H_2O)]^{3+}$-loaded NaY in argon up to 773 K leads to 100% autoreduction of rhodium and a formation of rather large rhodium particles. Large Rh particles are formed when Rh/NaY sample is reduced directly in H_2 confirmed by the lowest value of H/Rh

Table 1
H/Rh ratios obtained from TPD-H_2 for the samples after treatment by different activation procedures

Catalysts	Rh (wt.%)	Treatment	H/Rh
Rh/NaY-A	3	He (773 K)	0.18
Rh/NaY-H	3	H_2 (up to 673 K)	0.16
Rh/NaY-B1	3	O_2 (653 K), H_2 (673 K)	1.00
Rh/NaY-B2	3	O_2 (773 K), H_2 (673 K)	0.98
Rh/NaMOR-B1	3	O_2 (653 K), H_2 (673 K)	0.21
Rh/NaMOR^{N}-B1	3	O_2 (653, 673 K), NaOH	0.60
Rh/NaY-C	3	$CH_4/CO_2/N_2$	0.18
Rh/NaY^{N}-D	3	O_2 (653 K), H_2 (673 K), NaOH	0.90
Rh/NaY^{vap}-E	3	O_2 (653 K), H_2 (673 K), H_2/H_2O/He up to 973 K	0.42
Rh/NaY$^{N,\ vap}$-F	3	O_2 (653 K), H_2, NaOH, H_2/H_2O/He	0.41
Rh/NaY$^{N+H_2}$-G	3	O_2 (653 K), H_2 (673 K), NaOH, H_2 up to 673 K	0.90
Rh/NaY-B1	3	Used sample at 973 K	0.86
Rh/NaY^{N}-D	3	Used sample at 973 K	0.85
Rh/$Nb_2O_5^{vap}$-E	3	O_2 (653 K), H_2 (673 K), H_2/H_2O/He (773 K)	0.10
Rh/$Al_2O_3^{vap}$-E	1	O_2 (653 K), H_2 (673 K), H_2/H_2O/He (773 K)	0.40
Rh/TiO_2^{vap}-E	3	O_2 (653 K), H_2 (673 K), H_2/H_2O/He (773 K)	0.15

ratio of 0.16. Rh supported on mordenite also shows low H/Rh ratio before to be neutralized (Table 1).

The H/Rh ratio for Rh catalysts supported on oxide supports decreases in the following order: $Rh/Al_2O_3 > Rh/Nb_2O_5 > Rh/TiO_2$ (Table 1). The values of H/Rh ratios of these catalysts are lower compared to those of the zeolite-supported samples treated in O_2 and H_2 and neutralized, meaning a lower dispersion of the Rh particles on the amorphous supports.

3.4. ^{29}Si NMR spectra

^{29}Si NMR spectra of the initial NaY zeolite and spent NaY-supported Rh catalysts treated by different activation procedures are shown in Fig. 2A and B. Values of the framework Si/Al ratio for the spent catalysts are listed in Table 2. ^{29}Si NMR spectrum of NaY zeolite (Fig. 2A(a)) shows four peaks with chemical shifts (σ) at −104.5, −99.4, −93.5 and −87.9 ppm related to Si(0Al), Si(1Al), Si(2Al) and Si(3Al) environments, respectively with Si/Al ratio of 2.6. It is seen from Table 2 that Si/Al ratio of the zeolite framework structure of the samples is changed with the different procedures of treatment, as well as the intensities of peaks (Fig. 2). The samples treated in He, H_2 atmosphere and non-neutralized have a higher Si/Al ratio compared to that of the initial NaY zeolite (Fig. 2A(a) and (d) and Fig. 2B(a), (b) and (d)). This means a dealumination of the framework structure of NaY zeolite during reaction. With extent of the dealumination the intensities of the first peak, Si(0Al), and the second peak, Si(1Al) increase, while the intensities of the third peak, Si(2Al), and the fourth peak, Si(3Al), decrease. The highest value of Si/Al ratio of 3 is obtained for sample exposed directly to the conditions of reaction, suggesting a stronger dealumination (Table 2). Rh/NaMOR sample also exhibits higher Si/Al ratio value after reaction. However, the samples exposed to a neutralization of protons (Rh/NaY^{N}, Rh/NaY$^{N+H_2}$ and Rh/NaMOR^{N}) show similar Si/Al ratios to those of the initial NaY and NaMOR (2.6, 2.7 and 8.0, respectively; Table 2).

3.5. Catalytic activity data

Catalytic activity data for Rh catalysts supported on NaY zeolite and oxide carriers in the reaction of CO_2 reforming of CH_4 at 773 and 873 K temperatures are listed in Table 2. It is seen that the conversion of CH_4 and CO_2 is strongly influenced by the method of preparation and preliminary activation of the catalysts. Rh/NaY catalysts activated in He, H_2 and H_2/H_2O only and those submitted directly to the conditions of the reaction show very low conversions as well as a low specific activity (r). This phenomenon can be connected with both, the stronger dealumination

Table 2
Catalytic activity data of Rh-containing catalysts in CO_2 reforming of CH_4 at 773 and 873 K and Si/Al ratios

Catalysts	CH_4 conversion (%)	CO_2 conversion (%)	H_2/CO	r (mol CH_4/g Rh h)	Si/Al
Rh/NaY-A	5.0 (14.6)[a]	6.5 (17.7)	0.76 (0.81)	0.42 (1.22)	2.7[b], 3.0
Rh/NaY-H	3.6 (9.1)	4.7 (11.9)	0.78 (0.73)	0.30 (0.76)	2.8
Rh/NaY-B1	11.4 (35.0)	13.4 (35.6)	0.87 (0.89)	0.95 (2.92)	2.8
Rh/NaY-B2	12.2 (35.0)	12.5 (35.6)	0.97 (0.98)	1.02 (2.92)	2.7
Rh/NaMOR-B1	7.7 (–)	7.9 (–)	0.97 (–)	0.63 (–)	9.0
Rh/$NaMOR^N$-B1	9.7 (–)	10.6 (–)	0.99 (–)	0.84 (–)	8.0
Rh/NaY-C	5.3 (15.2)	6.6 (16.2)	0.79 (0.93)	0.45 (1.27)	3.0
Rh/NaY^N-D	9.0 (24.6)	9.6 (25.5)	0.93 (0.97)	0.75 (2.05)	2.6
Rh/NaY^N-D[c]	10.7 (–)	8.9 (–)	0.82 (–)	0.75	2.7
Rh/NaY^{vap}-E	5.1 (21.6)	6.4 (28.8)	0.76 (0.71)	0.43 (1.80)	2.8
Rh/$NaY^{N,\,vap}$-F	– (23.6)	– (32.7)	– (0.68)	– (1.97)	2.6
Rh/NaY^{N+H_2}-G	12.3 (–)	4.7 (–)	0.83 (–)	1.03 (–)	2.7
Rh/$Nb_2O_5{}^{vap}$-E	12.7 (–)	20.9 (–)	0.51 (–)	1.04 (–)	
Rh/$Al_2O_3{}^{vap}$-E	8.8 (–)	13.9 (–)	0.56 (–)	4.36 (–)	
Rh/$TiO_2{}^{vap}$-E	10.0 (–)	20.4 (–)	Nd	0.82 (–)	

Reaction conditions: 100 ml/min, $CH_4/CO_2/H_2$ (20/20/60), $m = 0.2$ g, $P = 1$ atm.
[a] At 873 K.
[b] Before to be used in reaction.
[c] Re-oxidated and re-activated after has been used in reaction.

of the zeolite framework and the agglomeration of rhodium particles confirmed by the ^{29}Si NMR (Fig. 2) and TPD-H_2 data (Table 1), respectively. Catalysts activated in oxygen, followed by hydrogen activation, and neutralized ones show the highest CH_4 and CO_2 conversions in CO_2 reforming of methane as well as the highest specific activity (Table 2). According to the different activation procedures, the specific activity of the zeolite-supported Rh catalysts decreases in the following order: Rh/NaY-B ≈ Rh/NaY^{N+H_2}-G > Rh/$NaMOR^N$-B1 > Rh/NaY^N-D > Rh/NaMOR-B1 > Rh/NaY-C > Rh/NaY^{vap} ≈ Rh/NaY-A > Rh/NaY-H. The activity of the neutralized catalyst, which after reaction was re-oxidated and re-activated, does not change (Table 2).

The conversions increase with increasing of the reaction temperature. It should be expected that the H_2/CO ratio be also increased. However, all catalysts at 773 and 873 K show H_2/CO ratio lower than 1 (Table 2), meaning that the thermodynamic equilibrium is not reached. However, for runs with a 0.200 g of catalyst at temperature about 973 K data of the equilibrium constant, K_p was close to the ratio $Q = P_{CO}^2 \times P_{H_2}^2 \times P_{CH_4}^{-1} \times P_{CO_2}^{-1}$. According to calculation related to partial pressures and temperature differences between bulk fluid and surface of the catalyst particle [21], any external mass and heat transfer were observed within our experimental conditions. It has been shown that TOF of Ru/NaY catalysts [6] as well as Ru catalysts supported on oxide supports, were very active in CO [5] and CO_2 hydrogenation [22].

It was suggested that a reverse water–gas shift reaction (WGSR) prevails at lower temperature in agreement with thermodynamics [23]. The measured H_2/CO ratios from Table 2 showed good agreement with those calculated by Eq. (1), presented by Bradford and Vannice [5] when the reaction equilibrium of production of synthesis gas from methane and carbon dioxide (2) is influenced by the simultaneous occurrence of the reverse WGSR (3):

$$\frac{H_2}{CO} = \left(3 - \frac{r_{CO_2}}{r_{CH_4}}\right)\left(1 + \frac{r_{CO_2}}{r_{CH_4}}\right) \quad (1)$$

$$CH_4 + CO_2 \Leftrightarrow 2CO + 2H_2 \quad (2)$$

$$CO_2 + H_2 \Leftrightarrow CO + H_2O \quad (3)$$

where r_{CH_4} and r_{CO_2} are the experimental rates of CH_4 and CO_2 conversions, respectively (Table 2).

If the observed TOF for the net rate of CO_2 reforming of CH_4 at 723 K, TOF_{obs}, is influenced by the

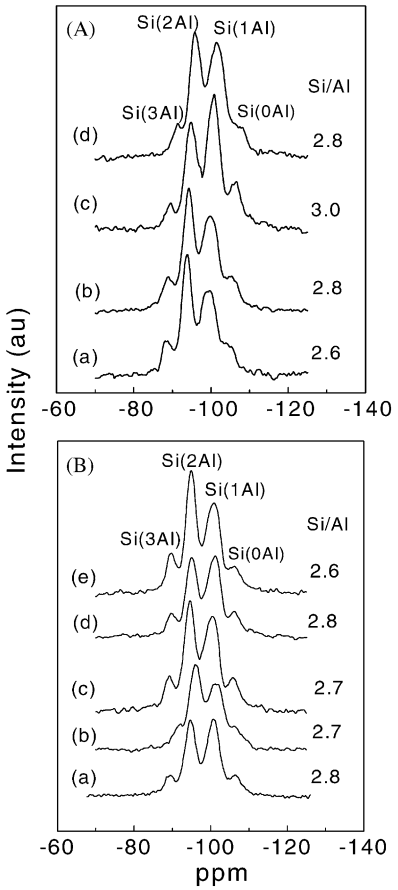

Fig. 2. ^{29}Si NMR spectra for zeolite-supported Rh catalysts treated by different activation procedures: (A) initial NaY zeolite (a), Rh/NaY-A (before to be used in reaction) (b), Rh/NaY-C (c) and Rh/NaY-H (d); (B) Rh/NaY-B1 (a), Rh/NaY-B2 (b), Rh/NaY^{N}-D (c), Rh/NaY^{vap}-E (d) and Rh/NaY$^{N,\,vap}$-F (e).

reverse reaction, the net rate can be approximated by the following expression [5]:

$$\mathrm{TOF_{obs}} = \mathrm{TOF_{for}} - \mathrm{TOF_{rev}} = \mathrm{TOF_{for}} - k_r P_{\mathrm{H_2}}^{\gamma} P_{\mathrm{CO}}^{\delta} \quad (4)$$

where $\mathrm{TOF_{for}}$ and $\mathrm{TOF_{rev}}$ are the turnover frequencies for the forward CO_2 reforming reaction of CH_4 (including the reverse WGSR) and for the reverse reaction (CO hydrogenation), respectively, k_r the rate constant for hydrogenation of CO, and P_{H_2} and P_{CO} are the partial pressures for H_2 and CO, respectively. The values of $\mathrm{TOF_{for}}$ and the kinetics parameters γ and δ obtained for $\mathrm{TOF_{CO}}$ according to Eq. (4) are summarized in Table 3. The dependence of TOF for CO formation on the partial pressures of CO and H_2 for different catalysts is, approximately linear as is shown on Fig. 3. The observed trend in $\mathrm{TOF_{CO}}$ with partial pressures of H_2 and CO shows an influence of the reverse reaction. This empirical analysis indicates that significantly high space velocities must be used to maintain low conversions which decrease effluent partial pressures H_2 and CO and thus minimize the influence of the reverse reaction during kinetic studies of CO_2 reforming of CH_4. The calculated values of k_r as well as the values of TOF for zeolite-supported Rh catalysts are much lower than those for oxide-supported ones (Table 3). It means that the influence of

Table 3
Kinetic data for catalysts obtained in the reaction of CO_2 reforming of CH_4 at temperature of 723 K

Catalysts	$\mathrm{TOF_{for}}$ CO (s^{-1})	k_r ($\mathrm{Torr}^{-(\delta+\gamma)}\,s^{-1}$)	δ	γ
Rh/NaMOR-B1	0.062	0.001	0.94	0.20
Rh/NaY-B1	0.055	0.001	0.81	0.20
4Rh/NaY-C	0.080	0.001	0.94	0.25
Rh/NaY^{N}-D	0.042	0.001	0.80	0.20
Rh/$Al_2O_3^{vap}$-E	0.520	0.036	0.12	0.81
Rh/$Nb_2O_5^{vap}$-E	0.480	0.005	0.71	0.25
Rh/TiO_2^{vap}-E	0.290	0.008	0.87	0.23

Reaction conditions: 100–400 ml/min, $CH_4/CO_2/N_2$ (20/20/60), $m = 0.2$ g, $P = 1$ atm.

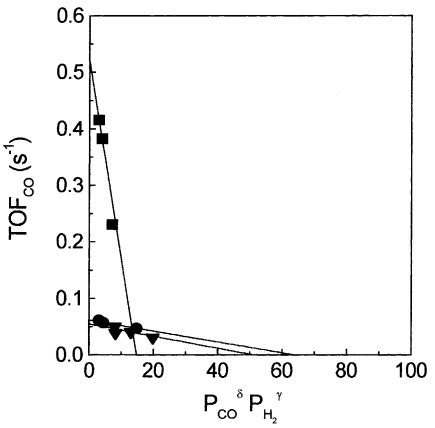

Fig. 3. TOF for carbon monoxide formation as a function of the effluent partial pressures of H_2 and CO at 723 K over Rh/$Al_2O_3^{vap}$-E (■), Rh/NaY-B1 (●) and Rh/NaMOR-B1 (▼).

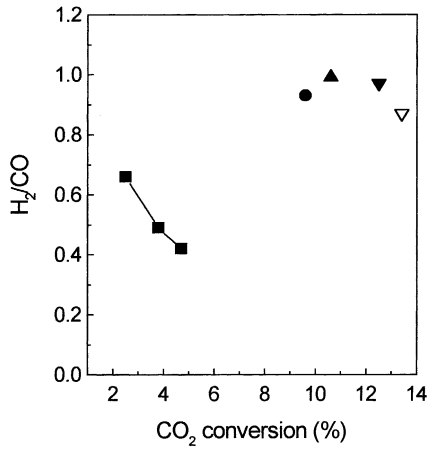

Fig. 4. Dependence of the H_2/CO product ratio on the carbon dioxide conversion for Rh/Al_2O_3 (■) at 723 K and for some Rh/NaY samples at 773 K: Rh/NaY-B1 (▽), Rh/NaY-B2 (▼), Rh/NaY^N-D (●) and $Rh/NaMOR^N$ (▲).

hydrogenation in kinetic studies is minimized for Rh zeolite catalysts.

It is seen from Table 2 that the values of CO_2 conversion are greater than those for CH_4 conversion, especially for oxide-supported Rh samples due to the influence of the reverse WGSR consisting with thermodynamic calculations. In addition, the values of measured H_2/CO ratio for the latter catalysts are significantly lower than 1. The H_2/CO product ratio determined during a series of activity tests is plotted as a function of carbon dioxide conversion for different samples in Fig. 4. The apparent relation between carbon dioxide conversion and the H_2/CO ratio indicates the strong influence of the water–gas shift equilibrium for oxide-supported Rh catalysts. This consists with results of Swaan et al. [24] and Blom et al. [25] who showed that H_2/CO is a function of water–gas shift equilibrium. For Rh zeolite catalysts the H_2/CO ratio are significantly higher compared to those for Rh catalysts over oxide carriers, suggesting that the influence of reverse WGSR is minimized (Table 2 and Fig. 4).

When the activity of the zeolite-supported catalysts in CO_2 reforming reaction is compared in terms of TOF_{for} (Table 3) the order of activity is the following: Rh/NaY-C > Rh/NaMOR-B > Rh/NaY-B > Rh/NaY^N-D. The order of activity compared by TOF for oxide-supported catalysts is as follows: Rh/Al_2O_3 > Rh/TiO_2 > Rh/Nb_2O_5 (Table 3).

There was a pronounced difference in the catalyst stabilities under reaction conditions. The activity of Rh catalysts supported on oxide supports decrease with time on stream, whereas all zeolite-supported Rh catalysts showed stable activity over reaction time of 300 h at 773 K. Although the high Si/Al ratios for Rh/NaY-C, Rh/NaY^{vap}-E, Rh/NaY-H and Rh/NaMOR samples, these catalysts showed remarkable stability in the activity under reaction conditions. Different opinions have been proposed about the unique stability of zeolite-supported noble metals [26,27]. Authors connect the high thermal stability with the dispersion of metal particles. However, Bath and Sachtler [23] have shown that the high thermal stability of Rh/NaY zeolite in CO_2 reforming of CH_4 was related to large Rh particles of 40 Å, which are formed in the initial stage of the catalytic operation: ones they are formed no further agglomeration takes place.

4. Discussion

4.1. Effect of the activation procedure on the structure and dispersion

The atmosphere of the primary thermal treatment strongly influences the rhodium particle size, consequently, the dispersion. The highest values of H/Me for Rh/NaY samples calcined at 653 or 773 K and followed by reduction at 673 K mean highly dispersed rhodium particles in NaY zeolite. Increasing of the temperature of calcination leads to a stabilization of the zeolite framework for Rh/NaY-B2 sample caused by the migration of the Rh^{3+} ions into the hexagonal prisms of zeolite. It is well known [20] that three types of rhodium species are formed in the reduced samples (after extended calcination at 773 K) identified as Rh^{3+} in supercages, Rh^+ in small cages and high temperature reduction species Rh^{3+} in hexagonal prisms. The reduction of the latter species will have higher activation energy than the reduction of the same ions in more accessible cages, where the concentration with lattice oxygen is less favorable. On the other hand, the small difference in the TPD data of both samples (Table 1) could be connected with the difference of the local environments of the rhodium particles on each of the samples. The slightly higher H/Me ratio for Rh/NaY sample calcined at lower

temperature may be is due to a multiple adsorption of hydrogen on rhodium atoms similar to the high H/Rh ratio reported for highly dispersed rhodium on alumina [20], where less than 10% of the rhodium present in a cationic form. It has been shown [28] that after calcination of Rh/NaY to 653 K, both RhO_2 and Rh_2O_3 were identified, besides small amounts of RhO^+ and Rh^{3+}. However, in the case of the Rh/NaY-B2 sample calcined at higher temperature most of the rhodium present in cationic form and some $[Rh_n^0 - H_x]^{x+}$ adducts would be formed as a result of reduction of rhodium cations to Rh^0 by reducible protons like to the observation by Tomczak et al. [20] for Rh/NaY calcined at 773 K. These adducts can agglomerate at high temperature (773 K) and to form small clusters of adducts, adsorbing less hydrogen. On the other hand, these samples show slowly dealumination of the zeolite framework (Table 2). It has been demonstrated [23] that non-neutralized Rh/NaY zeolite after use in the reaction of CO_2 reforming has rhodium particles of, approximately 40 Å and their formation inside the zeolite lead to some local destruction of the zeolite framework.

The lower values of H/Rh of the samples would be related to the suppression of H_2 chemisorption and/or growing of the metal particles according to the literature data. The H_2 chemisorption may be decreased due to metal particles filling of zeolite supercages. During the initial reduction of the precursor form of the catalyst, some of the rhodium may also have migrated to the external surface where large particles could be formed. Such distribution of metal particles between the pore system and the external zeolite surface has been demonstrated by TEM for Ru supported on zeolite [17]. On the other hand, the cause for the suppression of H_2 chemisorption can be the proton-adduct formation [17] that leads to a change of the electronic structure of the Ru clusters and this induces a lowering of the propensity of these particles to chemisorb hydrogen. A significant suppression of H_2 chemisorption can be occurred on Rh/zeolite due to an interaction of Rh with some zeolite hydroxyls [29].

For many catalytic reactions over zeolite-supported metal catalyst the zeolite protons can act as chemical anchors [30] for the metal particles in zeolite cages and stabilize the metal dispersion. However, the results indicate that the presence of protons and water producing during reverse WGSR destabilizes the dispersion of the metal particles, leading to favoring of the dealumination (Table 2). The very low values of H/Me ratios for the samples activated in steam, or H_2 atmosphere, or exposed directly to the reaction conditions can be connected with the formation of large metal particles. TEM and EXAFS analyses of rhodium in HY and NaY zeolites [23] were demonstrated, that a high concentration of protons within the zeolite has a dramatic effect on the size of particles formed during reduction. Probably, protons formed after autoreducing of $[Rh(NH_3)_5(H_2O)]^{3+}$ complex in Rh/NaY-C catalyst and then connected with H_2O produced during reverse reaction or liberated from inside of the zeolite provoke a high dealumination of the zeolite framework (Table 2). The effect of the hydrothermal treatment on the dealumination of zeolites is well known [31–33]. Dealumination through hydrothermal treatment leads to a hydrolysis of Al–O bonds with a creation of defect sites in the zeolite structure and the particles easily accumulate and aggregate in these sites under reaction conditions. Neutralization of the protons in Rh/NaY samples with NaOH suppresses the formation of large metal particles and stabilizes the zeolite framework under reaction (Rh/NaY^N-D, $Rh/NaY^{N,\,vap}$-F and $Rh/NaMOR^N$) as well as the surface of Rh particles to be accessible to the reagents (Tables 1 and 2). TEM analysis of Ru/NaY catalyst treated with $NaNO_3$ to neutralize protons after reduction was showed absence of any Ru metal particles larger than the zeolite Y supercage [17]. The importance of this neutralization to particle growth has been also documented for $[Pd(NH_3)_4]^2$/NaY [34].

4.2. Influence of the support on catalyst activity

Zeolite-supported Rh catalysts show a correlation of the CH_4 conversion and specific activity (r) with the accessible metal surface of the rhodium particles, as shown in Table 2. Increase of the metal dispersion leads to increase of the activity: Rh/NaY-B and neutralized Rh/NaY^N and Rh/NaY^{N+H_2} samples, having the highest dispersion, show the highest activity in CO_2 reforming of CH_4. Therefore, the influence of zeolite as support is limited to affecting the metal dispersion during the course of the catalyst preparation and stabilizing the metal surface area under reaction conditions, which is responsible for catalyst activity, similar to the inert SiO_2 support [26,27]. The same effect has

been found for zeolite-supported Ru catalysts in CO_2 reforming of CH_4 [6]. However, for oxide-supported catalysts there is no strong correlation between conversions and activity and the metal dispersion of Rh particles on the various supports (Table 2). It suggests that the activity of Rh catalysts supported on oxide supports depends on the type of the support: Rh supported on alumina shows the highest specific activity.

It should be noted, that the zeolite- and oxide-supported Rh catalysts differ in two main aspects: (i) the H_2/CO ratio is significantly higher for zeolite catalysts compared to that for amorphous-supported ones and (ii) the Rh zeolite catalysts reveal a significant stability with time on stream.

When the activity of the catalysts in CO_2 reforming reaction is compared in terms of TOF (Table 3) it is seen that the CO_2 reforming of CH_4 over oxide-supported Rh catalysts is coupled with reverse WGSR, which is quasi-equilibrated under reaction conditions. Experimental results indicate that the H_2/CO product ratio for oxide-supported Rh catalysts is a function of carbon dioxide formation (Fig. 4). Consequently, lower H_2/CO product ratio is obtained for these catalysts (Table 2). The kinetic data for Rh zeolite catalysts are not significantly influenced by the reverse reaction and the relative low values of TOF for Rh zeolite catalysts are likely due to the effect of the overall reverse reaction, which CO hydrogenation to CH_4 constitutes the initial reaction [5].

The difference in the catalytic behaviors of the samples could be strongly affected by the nature of the carrier, suggesting that the activity and rate of deactivation on metal particle size is likely to be related to the different extent of electronic interaction between metal and support, influencing the bonding and reactivity of the chemisorbed species [35,36]. It should be noted that the activity of Rh/Nb_2O_5 catalyst is high and similar to that of Rh/Al_2O_3 catalyst, while the rate constant for CO hydrogenation is very low and similar to that for Rh catalysts supported on NaY (Table 3). Therefore, it is reasonable to suppose that different mechanisms of activation of the reagents take place on the surface of the catalysts supported on Al_2O_3 and Nb_2O_5. It has been shown [37] that the CO chemisorption on Rh/Nb_2O_5 catalyst is suppressed by a geometric blockage of the Rh surface after high temperature reduction (773 K) due to more intimate contact between Rh and niobia that result in lower hydrogenation of CO. On the other hand, it is well known that partially reduced NbO_x species on the metal surface greatly promote catalytic activity in CO_2 reforming, because of the creation of a large number of interfacial sites [38].

Taking into account the small adsorption energy of CO_2 on Rh surface ($\approx$5 kcal/mol) [39] and the fact that dissociation of CO_2 on the surface of Rh is slower than dissociation of CH_4, the coverage of Rh with CO_2 will be very small at high temperature. According to Nakamura et al. [26] Al_2O_3 as support plays a role for accelerating of the CO_2 dissociation by rising CO_2 concentration in the vicinity of Rh particles by trapping CO_2 as formate, which produce CO after its decomposition. The electron transfer from the H to CO through Rh increases the Rh–C bond strength, and at the same time weakens the C–O bond on the surface that result in higher activity for CO hydrogenation [40]. Introduction of a strong metal-support interaction (SMSI) into Nb_2O_5- and TiO_2-supported metal catalysts can be also correlated with an increase of the electron density in the metal crystallites [41]. It cannot be excluded the acidic character of the carrier that may promote methane dissociation via CH^{3+} intermediate species on the sites at the perifering of the metal crystallites as was suggested by Huder [42] and Zhang et al. [43].

The TOF_{for} over more dealuminated zeolite-supported Rh catalysts are higher than those over less dealuminated catalysts (Table 3). Some diffusion effect inside the structure of zeolite could not be excluded, that causes the increase of activities of Rh/NaY-C and Rh/NaMOR samples with a higher degree of agglomeration of particles. Since the CO and H_2 has been reported to compete the same adsorption sites in CO hydrogenation [44], it is likely that a higher CO coverage on Rh decreases the concentration of hydrogen on the surface (i.e. H_2/CO decreases) and consequently the overall rate of the CO_2 reforming reaction on zeolite-supported Rh catalysts.

The absence of appreciable deactivation for zeolite catalysts during 300 h of time on stream is of importance for their industrial application. According to literature data different reasons would take place. The absence of coke formation as the main reason has been found for the extraordinary stability of zeolite-supported Rh catalysts. This can be related to some geometric effects caused by the microporous

structure of the zeolite, which inhibits the formation of coke. Another reason for the unusual stability of the zeolite catalysts is the absence of metal agglomeration during reaction. The small decrease of H/Me ratios for Rh/NaY-B1 and Rh/NaY^N-D samples (Table 1) (from 1.0 and 0.90 to 0.86 and 0.85, respectively) after they have been used in the reaction confirm the absence of a very strong sintering of the metal Rh particles during reforming process. Also, the Si/Al ratio values suggest no growth of particles beyond the size, which would lead to a drastic destruction of the zeolite framework. Dealumination of the zeolite framework does not proceed when the protons are neutralized and it leads to increase of the CH_4 conversion and specific activity of the zeolite catalyst (Table 2).

The thermal stability of oxide-supported catalysts is affected by the dispersion of metal particles. Rh catalyst supported on alumina with high dispersion (Table 3) exhibited higher thermal stability compared to that for niobia- and titania-supported catalysts.

The different behaviors of both Rh series catalysts with respect to carbon deposition reflects different mechanistic processes occurring for the reforming of CH_4 with CO_2 depending on the nature of the support used. The deactivation of the oxide-supported catalysts could be related to the long residence time of the carbonaceous intermediates on the metal surface, which favor polymerization and eventually formation of graphitic-type carbon on the Rh particles. It has been shown for alumina-supported ruthenium catalyst [27] that the surface hydroxyl groups in the oxide are responsible for the diffusion process that allow mobility of oxygen and hydrogen, thus increasing the resistance to carbon deposition by oxidation of the carbonaceous adsorbed species formed from methane adsorption on the metal.

The relative catalyst resistance to coking for oxide-supported Rh catalysts is $Rh/Al_2O_3 > Rh/Nb_2O_5 > Rh/TiO_2$, which would be correlated with the support ability to stabilize CH_x decomposition and carbon monoxide dissociation [45]. It should be noted that the initial activity of Rh supported on TiO_2 was very high, but quickly deactivation after few hours was observed. We suppose that due to SMSI phenomenon TiO_x species are formed, which promote the high initial activity. The strong deactivation of Rh/TiO_2 catalyst may be due to either continual deposition of carbon or additional blockage of active sites by migrating TiO_x species under reaction conditions and the activation barrier for methane dissociation increases [41]. On the other hand, the presence of large quantities of water formed during reverse WGSR may produce surface hydroxyl groups via dissociation of water that leads to a decomposition of formate-type intermediate CH_xO species, which yield H_2 and CO at the metal-support interface [41,45].

5. Conclusions

Two groups of catalysts are formed according to the procedure of the catalyst activation: (i) non-neutralized and (ii) neutralized. Non-neutralized samples suffer a partial destruction of zeolite structure after reaction. Neutralization of the protons leads to a stabilization of the zeolite framework.

A correlation between the specific activity in CO_2 reforming and the dispersion of metal particles for Rh/NaY zeolites is revealed. TOF for CO formation over supported Rh catalysts are strongly affected by the type of the support. The activity of oxide-supported Rh catalysts is mainly determined by the participation of the reverse WGSR. Zeolite-supported Rh catalysts reveal a strong thermal stability.

Acknowledgements

The authors gratefully acknowledge the financial support of Fundação para o Amparo a Pesquisa do Estado de São Paulo (FAPESP), Financiadora de Estudos e Projetos (FINEP) and Conselho Nacional de Desenvolvimento Cientifico e Tecnológico (CNPq).

References

[1] J.R. Rostrup-Nielsen, J.H. Bak Hansen, J. Catal. 144 (1993) 38.
[2] M.F. Mark, W.F. Maier, J. Catal. 164 (1996) 122.
[3] P. Gronchi, P. Centola, R. Del Rosso, Appl. Catal. A: Gen. 152 (1997) 83.
[4] M.E.S. Hegarty, A.M. O'Cornner, J.R.H. Ross, Catal. Today 42 (1998) 285.
[5] M.J.J. Bradford, M.A. Vannice, J. Catal. 183 (1999) 69.
[6] U.L. Portugal, C.M.P. Marques, E.C.C. Araujo, E.V. Morales, M.V. Giotto, J.M.C. Bueno, Appl. Catal. A: Gen. 193 (2000) 173.
[7] A.M. Cadalla, M.E. Sommer, Chem. Eng. Sci. 44 (1989) 2825.

[8] B. Delmon, Appl. Catal. B 1 (1992) 139.5.
[9] J.D. Fish, D.C. Hawn, J. Sol. Energy Eng. 109 (1987) 215.
[10] A.M. Gadalla, M.E. Sommer, Chem. Eng. Sci. 44 (1989) 2825.
[11] T. Osaki, T. Horuchi, K. Suzuki, T. Mori, Catal. Lett. 29 (1995) 39.
[12] S. Wang, G.Q. Lu, Appl. Catal. B: Environ. 19 (1998) 267.
[13] J.A. Montoya, E. Romero-Pascual, C. Gimon, P. Del Angel, A. Monzon, Catal. Today 63 (2000) 71.
[14] A.T. Ashcroft, A.K. Cheethan, M.L.H. Green, P.D.F. Vernom, Science 352 (1991) 225.
[15] J.R. Rostrup-Nielsen, Stud. Surf. Sci. Catal. 81 (1994) 25.
[16] Z.L. Zhang, V.A. Tsipouriari, A.M. Efstathiou, X.E. Verykios, J. Catal. 158 (1996) 51.
[17] T.J. McCarthy, C.M.P. Marques, H. Treviño, W.M.H. Sachtler, Catal. Lett. 43 (1997) 11.
[18] E. Lippmaa, M. Mägi, A. Samoson, G. Engelhardt, A.R. Grimmer, J. Am. Chem. Soc. 102 (1980) 4889.
[19] J. Klinowski, S. Ramdas, J.M. Thomas, J. Chem. Soc., Faraday Trans. 78 (1982) 1025.
[20] D.C. Tomczak, G. D Schünemann, H. Treviño, W.M.H. Sachtler, Microporous Mater. 5 (1996) 263.
[21] G.F. Froment, K.B. Bischoff, Chemical Reactor Analysis and Design, Wiley, New York, 1990.
[22] S. Scire, C. Crisafulli, R. Maggiore, S. Munico, Catal. Lett. 51 (1998) 41.
[23] R.N. Bath, W.M.H. Sachtler, Appl. Catal. A: Gen. 150 (1997) 279.
[24] H.M. Swaan, V.C.H. Kroll, G.A. Martin, C. Mirodatos, Catal. Today 21 (1994) 571.
[25] R. Blom, I.M. Dahl, A. Slagtern, B. Sortland, A. Spjelkavik, E. Tangstad, Catal. Today 21 (1994) 535.
[26] J. Nakamura, K. Aikawa, K. Sato, T. Uchijima, Stud. Surf. Sci. Catal. 90 (1993) 95.
[27] P. Ferreira-Aparicio, I. Ridriguez-Ramos, J.A. Anderson, A. Guerrero-Ruiz, Appl. Catal. A: Gen. 202 (2000) 183.
[28] V. Schünemann, B. Adelman, W.M.H. Sachtler, Catal. Lett. 27 (1994) 259.
[29] H.T. Wang, Y.W. Chen, J.G. Goodwin, Zeolites 4 (1984) 56.
[30] L. Xu, L. Sachtler, Adv. Catal. 39 (1993) 139.
[31] T.H. Fleisch, B.L. Meyers, G.J. Ray, J.B. Hall, C.L. Marshall, J. Catal. 99 (1986) 117.
[32] Th. Gross, U. Lohse, G. Engelhardt, K.H. Richter, V. Patjelova, Zeolites 4 (1984) 25.
[33] Q.L. Wang, G. Giannetto, M. Torrealba, G. Perot, C. Kappenstein, M. Guisnet, J. Catal. 130 (1991) 459.
[34] S.T. Homeyer, W.M.H. Sachtler, J. Catal. 117 (1989) 91.
[35] S. Scire, C. Crisafulli, R. Maggiore, S. Minico, S. Galvagno, Catal. Lett. 51 (1998) 41.
[36] F. Solymosi, I. Tombacz, M. Kocsis, J. Catal. 75 (1982) 78.
[37] M.C.J. Bradford, M.A. Vannice, Catal. Lett. 48 (1997) 31.
[38] S.I. Ito, T. Fujimori, K. Nagashima, K. Yuzaki, K. Kunimori, Catal. Today 57 (2000) 247.
[39] W.H. Weinberg, Surf. Sci. 128 (1983) 2224.
[40] M.A. Vannice, J. Catal. 40 (1975) 129.
[41] M.C.J. Bradford, M.A. Vannice, Appl. Catal. A: Gen. 142 (1996) 73.
[42] K. Huder, Chem. Eng. Tech. 63 (1991) 376.
[43] Z.L. Zhang, X.E. Verykios, M. Baerns, Catal. Rev. Sci. Eng. 36 (1994) 507.
[44] I.A. Fisher, A.T. Bell, J. Catal. 54 (1996) 162.
[45] M.C.J. Bradford, M.A. Vannice, Appl. Catal. A: Gen. 142 (1996) 97.